Arab J Sci Eng (2013) 38:817–828
DOI 10.1007/s13369-012-0521-x

RESEARCH ARTICLE - CIVIL ENGINEERING

Theoretical and Experimental Analysis of Wave Impact Pressures on Curved Seawalls

Mustafa Mamak · Hasan Guzel

Received: 4 February 2011 / Accepted: 15 May 2011 / Published online: 10 January 2013

Abstract Experimental model tests were performed in a wave flume with regular waves to measure the magnitude and distribution of impact pressures caused by breaking waves on a curved seawall model having different radii of curvatures. The base structure of the wall has a foreshore slope of 1/10. Theoretical studies based on pressure impulse theory were carried out to obtain the numerical results of breaking wave impact pressures on curved seawalls. The boundary element method was used for the numerical solution of the governing equation. The novel aspect of this study was to investigate the applicability of pressure impulse theory to curved seawalls. The results showed that the pressure impulse model can be used to model the wave impact pressures and their distribution on curved seawall models with good accuracy. A slight decrease has been observed in pressures for increasing radii of curvatures, especially for the case which the water depth at wall was 14 cm. The location of the maximum impact pressure was found to occur above the still water level for all cases tested in this study.

Keywords Breaking wave · Coastal engineering · Curved seawall · Pressure impulse · Wave impact pressure

الخلاصة

لقد أجريت اختبارات أنموذج تجريبية في وهد موجي مع موجات منتظمة لقياس حجم وتوزيع الضغوط الناجمة عن تأثير موجات كاسرة في أنموذج سور بحري منحن له أنصاف أقطار مختلفة من التقوسات. ولهيكل الجدار الأساسي ميل شواطئ أمامية بمقدار 1/10. وقد أجريت الدراسات النظرية على أساس نظرية الضغط الدافع من أجل الحصول على النتائج العددية لتأثير ضغوط الموجات الكاسرة على الحوائط البحرية المنحنية واستُخدمت طريقة العنصر المحدود من أجل الحل العددي لمعادلة التحكم. والجانب غير المألوف من هذه الدراسة هو التحقيق في تطابق نظرية الضغط الدافع مع الحوائط البحرية المنحنية. وأظهرت النتائج أن أنموذج الضغط الدافع يمكن أن يستخدم لنمذجة تأثير ضغوطات الموجة وتوزيعها على نماذج السور البحري المنحني بدقة جيدة. لقد لوحظ انخفاض طفيف في الضغوط كعبرة لزيادة الانحرافات، وبخاصة بالنسبة للحالة التي فيها عمق الماء في الجدار أربعة عشر سنتيمتر. وعثر على أن موقع تأثير الضغط الأقصى يحدث فوق مستوى المياه الساكنة (SWL) لجميع الحالات المختبرة في هذه الدراسة.

1 Introduction

Seawalls and breakwaters have been widely used as shore protection structures to stabilize the shore against wave action. These structures near the shoreline are subject to impulsive wave pressures, which are high in magnitude and short in duration, when impacted directly by breaking waves. The impulsive wave pressures induced by breaking waves are much greater than the ones measured due to non-breaking waves. The maximum peak pressures were of the order 10 $\rho g(d_w + H_b)$ [1], where ρ is the density of water, g is the acceleration of gravity, d_w is the water depth in front of the structure, and H_b is the breaking wave height. The impact pressures and especially maximum pressure region are significant for determining the terms of stability and safety of the structure. The interactions between breaking waves and structure may result in very complex flow fields. Therefore, it is necessary to obtain these pressures and their distributions

M. Mamak (✉)
Department of Civil Engineering,
Abdullah Gul University, Kayseri, Turkey
e-mail: mustafa.mamak@agu.edu.tr

H. Guzel
Department of Civil Engineering,
Mustafa Kemal University, Hatay, Turkey
e-mail: hguzel@mku.edu.tr

on the wall to be able to design structures strong enough to withstand wave effects.

Many experimental and theoretical studies concerning impact pressures on seawalls and the shape of the breaking wave in the presence of structures are reported in the literature. Measurements of full-scale wave impact pressures on seawalls have been made by Blackmore and Hewson [2]. History and spatial distribution of impact pressures on vertical [3–5] and sloping [6,7] plane seawalls has been determined by laboratory experiments. Simultaneous measurements of the kinematics and dynamics of impact show that impact occurs through the focusing of the incident wave front onto the wall, trapping some amount of air in the process [4]. Simple prediction methods are proposed to estimate the wave-induced pressures on smooth impermeable seawalls [8]. Bullock et al. [9] found that the peak impact pressures tended to be higher and the rise times shorter with freshwater waves than with geometrically similar seawater waves. Even for series of supposedly regular waves, there is great variability in the violence of the impacts. This is due to the shape of the breaker having an important influence on the impact pressures [10]. The numerical results of the impact pressures on vertical wall from the pressure impulse model [11] are found to agree well with the experimental data [7].

Bagnold [12] and Richert [13] showed that the impulse given by a wave is much more consistent than force or pressure in measuring the impact of a wave. Experimental studies confirming the value of the pressure impulse approach are described by Chan [14], who shows that the concept is useful within its limitations.

Goda [15] has recommended a conservative method for breaking wave force determination, but this method may underestimate the wave force. A formulation has been given for the motion of an upright section of composite breakwater activated by an impulsive force due to breaking waves [16]. Goda [17] has reviewed his formula and discussed on the possibility of the generation of impulsive wave force and its treatment in breakwater design.

A large data set has been investigated to predict horizontal wave forces on vertical breakwaters [18]. Allsop et al. [19] showed that impulsive breaking is particularly severe for steep or vertical walls with steep beaches.

Müller and Whittaker [20] have compared the two formulas recommended by the Coastal Engineering Research Center and by the British Standard Institution for the calculation of wave impact pressures with respect to the magnitudes of the design pressures as determined for given situations.

Kortenhaus and Oumeraci [21] have investigated the complexity of wave behaviour experimentally in front of a vertical breakwater. Goda [22] developed overtopping guidelines based on prototype investigations consisting of wave climate measurements and expert impressions of the impact of overtopping volumes on different objects situated on top of breakwaters. Cuomo and Allsop [23] have reported recent advances in knowledge on impulsive wave loads on vertical/steep walls.

A detailed research programme has investigated a non-wave overtopping seawall which has a large radius curve starting well below still water level (SWL) whose radius changes with elevation. Results of regular wave tests and numerical simulations are given in Kamikubo et al. [24], and new irregular wave data has been presented by Yamashiro et al. [25].

Compressibility seems to be important in wave impacts only when air is trapped in the water. The larger the amount of the entrapped air at impact, the lower the magnitude and the longer the rise or compression time of the impact pressures [26]. However, it is shown that a high level of aeration does not always reduce the peak pressure, although it tends to increase both the rise time and duration [27].

Use of model tests includes analysis of scale effects. Wave impacts in small scale hydraulic model tests are greater in magnitude, but shorter in duration than their equivalents at full scale in seawater, so simple Froude scaling will over-estimate prototype loads, but under-estimate their durations.

Many investigators using the pressure impulse model calculated theoretical impact pressures due to the whole time of impact. However, Peregrine [1] and Kirkgöz and Mamak [11] have considered the impact to be only due to the violent peak, not the total time that the wave crest spends at the wall. This suggestion seemed more appealing to us and we have computed the theoretical impact pressures using t_m, which is the time interval between the impact pressure first begins to act and the pressure reaches its peak value. The computational results of the impact pressures from the pressure impulse model using this assumption were found to agree well with the experimental data of an earlier study [6].

Wood et al. [28] used a theoretical pressure impulse model to compare with experimental pressure measurements for breaking waves impacting on a vertical wall. They showed that pressure impulse theory has the advantage of providing simple Fourier solutions to complex situations. These solutions are quick to evaluate, and from the study, it was shown that they can be reasonably accurate.

The concept of performance design is new, and can be considered as a design process that systematically defines performance requirements and respective performance evaluation methods. Expected sliding distance method was proposed by Shimosako and Takahashi [29]. They called it "deformation-based reliability design method" which integrated the Monte Carlo technique and the stochastic behaviours of design factors.

There are rare studies on curved seawalls, and the impact pressures reported are very different in magnitude and seem to be dependent on many parameters such as wave, geometry and boundary conditions. The pressure impulse theory seems

to be able to predict impact pressures reasonably well, but has not yet been applied to curved walls. Therefore, in this study, experimental investigations were performed in a wave flume with regular waves to obtain the magnitude and distribution of impact pressures induced by breaking waves on curved seawalls having different radii of curvatures. A theoretical approach based on the pressure impulse theory was used to compute the theoretical impact pressures on curved seawall models. A comparison between experimental data and computational results obtained by the boundary element method is presented, and the location of maximum impact pressure is analysed.

2 Experimental Setup and Procedure

The experimental investigations were conducted in a wave flume at the Laboratory of Hydraulic Research Centre of Railway, Harbour and Airport General Directorate, Ankara, Turkey. The flume is 40 m long, 0.60 m wide and 1.20 m deep. Regular waves were produced by a paddle-type wave generator located at one end of the flume. A wave absorber was installed at the other end of the flume. Figure 1 shows a schematic diagram of the wave flume with the curved seawall model. The foreshore slope for the experiments was set at 1/10, following findings from Carr [30], Richert [13] and Kırkgöz [5] that the greatest maximum pressures are found to occur on this slope.

In the experiments, four wave probes were used to measure the wave profile as shown in Fig. 1. The wave height, H, was determined by zero down-crossing method taking the averaged values obtained from the two probes placed near to the wave generator, because the wave characteristics change on the sloping part of the base structure while approaching to the wall. Total number of waves was 36 for each water depth (d_w) in front of the wall, and repeated for seawall models. In order to prevent the reflection of the waves, a wave absorber was used, and the number of waves generated by the paddle was limited to 6 or 7 for a run. The horizontal distance between the wave generator and the base structure of seawall, where the 1/10 slope begins, is 20 m. The length of the base part is 6 m. The curved seawall models were located at a distance of 14 m from the other end of the wave flume.

The water depth (d_w) in front of the wall affects the breaking process of a particular wave. The water depth and the location of the wave plunging point were determined in order to have a perfect impact, because the presence of a structure causes a slight horizontal shift shoreward in the location of the breaking point by affecting the geometry of the plunging breaker [7]. For this reason, a series of preliminary tests where the water level in front of the wall was changed within the range of 10–20 cm were conducted to obtain the depths at which the greatest pressures occurred on the curved seawall models. Having fixed this water depth, a particular experiment was repeated several times under the same conditions until an adequate number of impact data was available. About 45 min was allowed between the individual runs for the surface disturbances in the flume to die out. With regard to the magnitude, the impact pressure data which have so far been collected in both the laboratory and the field show extreme variations, even when all waves are identical. Therefore, nearly 2,000 waves had been used to obtain impact pressure data. For each test case, 144 of total waves showing impact characteristics were used for the analysis.

The breaking wave heights (H_b) for all test conditions were obtained during experiments from the records of a Sony TRV 320E video camera. By analysing the video records frame by frame, the breaker height (H_b) of experimental impact pressures was determined. The number of frames per second was 24. Table 1 shows the total number of waves used for each test, water depths at walls (d_w), wave heights near to the wave paddle (H), and breaking wave heights (H_b) used in the experiments. Three different water depths have been used depending on the water depth at wall. The small range of the parameters depends on the impact and wave overtopping condition. When the water depth at wall was lower than 14 cm, impact pressures could not be obtained, and when d_w was higher than 17 cm, wave overtopping occurred. This was the reason for the small range of parameters. The wave period was kept constant throughout the experiments ($T = 2$ s), and as a result, only one steepness of regular waves within the breaker range was produced. The reason for having only one steepness is because it was found that for the same

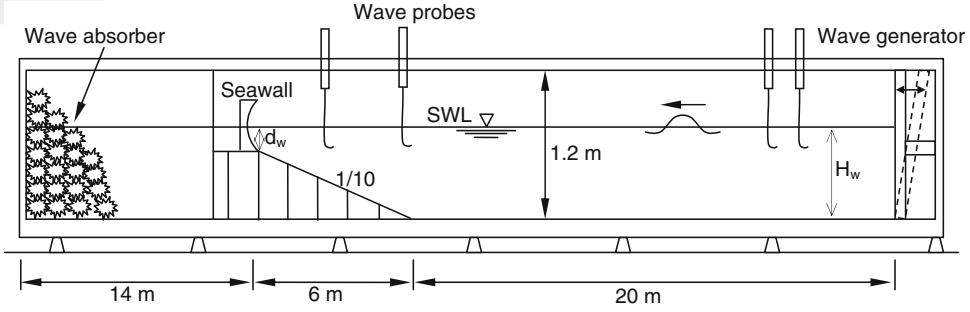

Fig. 1 Schematic diagram of the wave flume with the curved seawall model

Table 1 Experimental conditions

Test no.	Total number of waves	Water depth at wall, d_w (cm)	Wave height near to paddle, H (cm)	Breaking wave height, H_b (cm)	Wave period, T (s)
Test 1	144	14	18	13	2
Test 2	144	15	19	14	2
Test 3	144	17	21	16	2

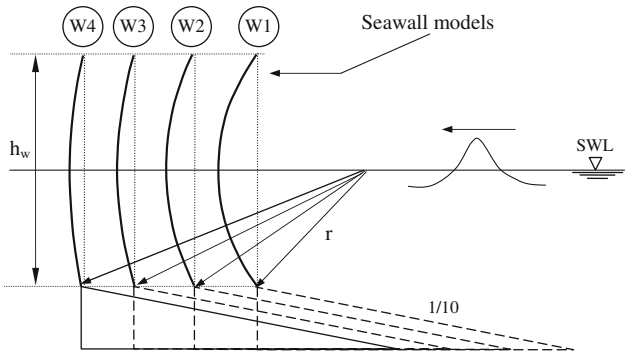

Fig. 2 Seawall models

foreshore slope, the wave steepness has very little influence on the magnitude of the dimensionless impact pressures [5].

Four seawall models (W1, W2, W3, and W4) having different radii of curvatures ($r = 30, 40, 60$, and 80 cm, respectively) were made of sheet iron and fixed at the top of the base structure (Fig. 2). The height of the all walls was same and set at $h_w = 40$ cm. The top and the bottom of the walls were placed in the same vertical direction, so that they are all symmetrical with respect to middle part of the walls.

Impact pressures were measured by seven 10 mm transducers located vertically along the wall centerline (Fig. 3). The pressure transducers were Kenek model P310-1 type, and each having an operating pressure of 14.2 psi (98.1 kN/m^2), with 150 % overload capability and a natural frequency of 9.1 kHz. The sample frequency of measurements was 5 kHz. The lowest transducer on the wall was 20 mm from the bottom. The details of the location of the pressure transducers from the bottom of the seawall model are given in Fig. 3.

A typical pressure history resulting from a transducer is seen in Fig. 4. In this figure, the maximum value of the pressure is denoted by p_m and is referred to as the impact pressure. The larger the amount of the entrapped air at impact, the lower the magnitude and the longer the rise or compression time of the impact pressures [26]. In the present study, it was not possible to determine accurately the dimensions of an air pocket. However, it was observed during video analysis that the greatest impact pressures occurred when the breaking wave trapped a very thin pocket of air. Table 2 gives the dimensionless maximum impact pressures ($p_{max}/\gamma H_b$) of some previous investigations and the present study in terms of average and maximum values for regular and random waves.

It is seen that the impact pressures of the present study are higher than some of the previously reported ones. However, McKenna and Allsop [31] have reported significantly higher normalised pressures.

As may be noted from Table 2, the average dimensionless pressures obtained for the curved wall are in the range of the values reported from other model studies. Highest values of field and prototype experiments are greater than the present study, except for the field study of Blackmore and Hewson [2]. Moreover, Kirkgöz and Mamak [11] showed that the dimensionless maximum impact pressure ($p_{max}/\gamma H_b$) was 40 for a vertical wall, and this value is nearly two times greater than the dimensionless maximum impact pressure ($p_{max}/\gamma H_b = 17.5$) obtained in the present study for a curved wall.

3 Theoretical Analysis

Wave impact phenomenon on a wall can be formulated using one-dimensional Euler's equation of motion of incompressible inviscid fluid flow. That is, for the present case ignoring the nonlinear convective terms and viscosity, the governing equation of the motion in horizontal direction may be written as

$$\frac{\partial \vec{u}}{\partial t} = -\frac{1}{\rho}\vec{\nabla} p \tag{1}$$

where $\vec{u}$ is the horizontal flow velocity, $p(x, y, t)$ is the impact pressure, ρ is the density of water, x is the coordinate axis in the horizontal direction, y is the coordinate axis in the vertical direction and t is the time.

It may be assumed that the whole horizontal momentum of the virtual mass involved in the impact process is exchanged between the time the impact pressure first begins to act and the time, t_m, the pressure reaches its peak value, p_m [1,11]. Then, during this time interval, the flow velocity changes between U_b which corresponds to the wave approach velocity at breaking point, and U_a after the impact. U_b is taken to be uniform for simplicity as suggested by Cooker and Peregrine [32]. The component of velocity U_a, in the direction normal to the wall is assumed to be zero after impact. Here, impact term refers to the rise time. However, if a horizontal velocity was existed, it would not make any difference

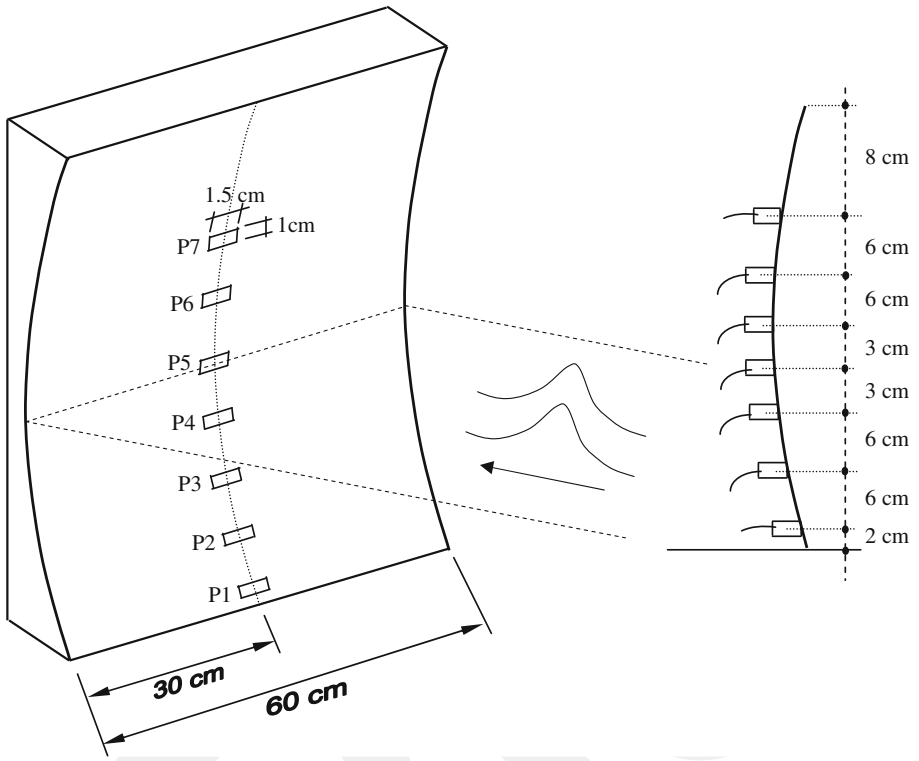

Fig. 3 The details of the location of the pressure transducers

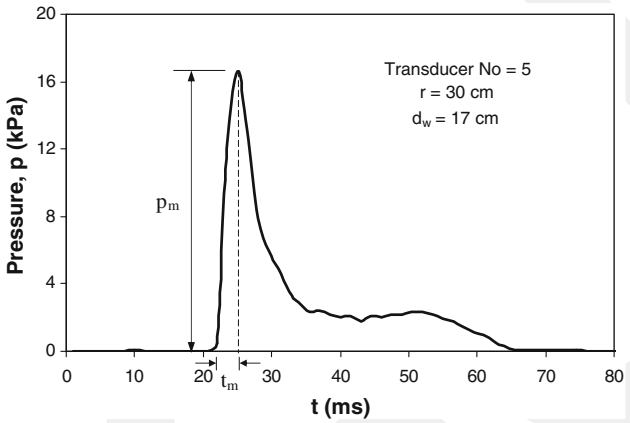

Fig. 4 A typical pressure history from one of the transducers

for Eq. 5, because the divergence of Eq. 4 was taken and the differential equation called Laplace equation was obtained.

Now integrating Eq. 1 with respect to time between $t = 0$ and $t = t_m$:

$$\int_0^{t_m} \frac{\partial \vec{u}}{\partial t}\,dt = -\frac{1}{\rho}\vec{\nabla}\int_0^{t_m} p(t)\,dt \tag{2}$$

in which the pressure impulse, P, is defined by

$$P = \int_0^{t_m} p(t)\,dt \tag{3}$$

Using Eq. 3, integration of Eq. 2 gives

$$\vec{U}_b - \vec{U}_a = \frac{1}{\rho}\vec{\nabla} P \tag{4}$$

Taking the divergence of Eq. 4, the following differential equation is obtained:

$$\nabla^2 P = 0 \tag{5}$$

Equation 5 shows that the pressure impulse satisfies the Laplace's equation.

The right-hand side of Eq. 3 may be estimated by assuming that the relationship between $p(t)$ and t is linear during the time interval, t_m, i.e., $P = p_m t_m/2$ which gives the impact pressure as

$$p_m = \frac{2P}{t_m} \tag{6}$$

Once the pressure impulse, P, is solved from Eq. 5, the impact pressure, p_m, can be determined if the rising time of the pressure, t_m, is known in Eq. 6.

The analytical solution of Eq. 5 for problems of solution domains having simple geometries was presented by Cooker and Peregrine [32]. In the following, the numerical solution of Eq. 5 is given that is applicable to any shape of solution domains.

Table 2 Dimensionless impact pressures from some of the previously reported and present studies

Author	Type of experiment	Type of wall	$p_{max}/\gamma H_b$	
			Average	Highest
Rouville et al. [33]	Field	Plane	–	28
Nagai [34]	Model	Plane	11	20
Mitsuyasu [35]	Model	Plane	20	35
Kirkgöz [36]	Model	Plane	15	–
Blackmore and Hewson [2]	Field	Plane	2.3	5.5
Partenscky [3]	Prototype	Plane	–	27
McKenna and Allsop [31]	Model	Plane	–	50
Present study	Model	Curved	13.5	17.5

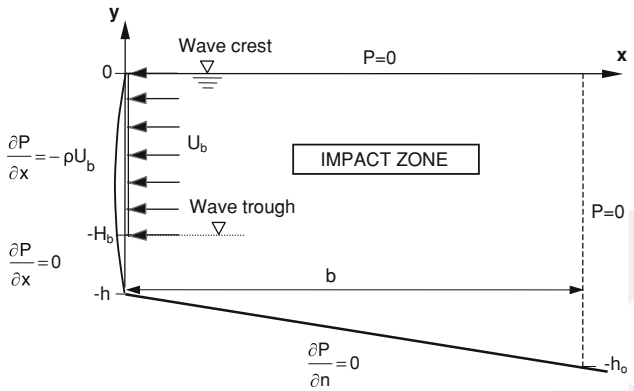

Fig. 5 Idealized model of wave impact on curved wall

3.1 Idealized Wave Impact Model

The numerical solution of Eq. 5 is applied to the idealized model of wave breaking on a curved wall shown in Fig. 5. As may be seen from the figure, the solution domain of the numerical model for the impact zone of flow extends from the rigid curved wall with depth, h, to a water depth of h_0, and the width b of the idealized impact zone. Mamak [37] showed that the pressure impulse, P, increases with increasing width, b. However, it is found that b is no more effective on P, when $b \geq 10h$. So, the value of $b = 10h$ is used in the numerical computations. The upper boundary of the problem is represented by the breaker crest elevation and the lower boundary is the sea bed. Along the breaker height H_b, the wall is exposed to direct wave impact. In this model, the left and lower boundaries of the problem, that is the face of the wall and the bed profile may have any type of geometric configuration.

3.2 Boundary Conditions

The boundary conditions of the impact model in Fig. 5 are given below. For upper and right-hand edges:

$$(P)_{y=0} = 0 \quad \text{and} \quad (P)_{x=b} = 0 \tag{7}$$

$P = 0$ on the free surface, when pressure is measured relative to atmospheric pressure. Far from the impact region, P is taken to be zero.

For left-hand edge:

$$\text{Over the impact region}: \left(\frac{\partial P}{\partial x}\right)_{x=0} = -\rho U_b \tag{8}$$

$$\text{Below the impact region}: \left(\frac{\partial P}{\partial x}\right)_{x=0} = 0 \tag{9}$$

where liquid meets a solid boundary during impact, the change in normal velocity gives the normal derivative of pressure impulse.

At the lower edge, the normal velocity is unchanged so that:

$$\frac{\partial P}{\partial n} = 0 \tag{10}$$

In Eq. 8, the fluid velocity at the instant of impact is taken equal to the wave celerity which is approximately defined as $U_b = (gh)^{1/2}$.

The governing equation of the model, Eq. 5, can be solved for P, subject to the boundary conditions given by Eqs. 7–10.

4 Numerical Solution

The numerical solution of Eq. 5 was carried out using the methods of finite difference, finite element and boundary element [37]. The comparison of the numerical and analytical results for P on the vertical wall of a simple rectangular impact zone showed that the boundary element method produces the nearest values to the analytical results with the shortest computing time. Therefore, in this study, the boundary element method is used for the numerical computations.

The boundary element method is briefly outlined below. The constant elements chosen on the boundary, Γ, of the solution domain and the nodes representing the middle points of these elements are shown in Fig. 6. The number of elements

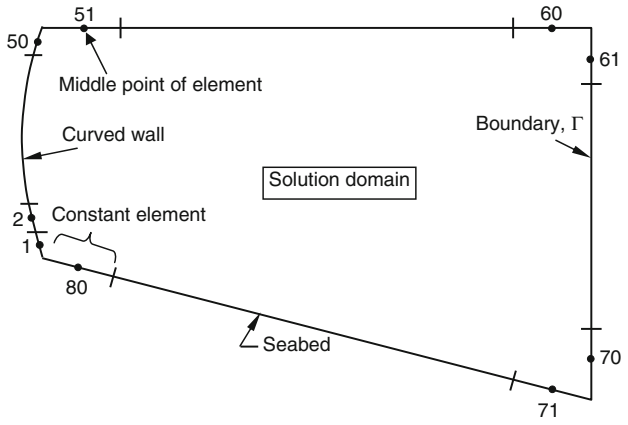

Fig. 6 Boundary elements of the solution domain

on the wall boundary is increased in order to compute the pressure impulse on the wall more precisely.

If the boundary integral equation is applied to the pressure impulse given by Eq. 5,

$$cP + \int_{\Gamma} P \frac{\partial w}{\partial n}\,\mathrm{d}\Gamma = \int_{\Gamma} \frac{\partial P}{\partial n}\, w\,\mathrm{d}\Gamma \tag{11}$$

where c is a coefficient depending on the shape of the boundary and w is the fundamental solution of Laplace equation [38]. For constant type of element, the boundary is always 'smooth' as the node is at the centre of the element, hence the value of c is 1/2. For an isotropic domain, the fundamental solution of Laplace equation is

$$w = \frac{1}{2\pi} \ln\left(\frac{1}{r}\right)$$

where r is the distance from the point of application of the delta function to any point under consideration.

Equation 11 may be written for a given point "i" and can be discretized for all the elements along the boundary, that is

$$\frac{1}{2} P_i + \sum_{j=1}^{n} \left(\int_{\Gamma_j} \frac{\partial w}{\partial n}\,\mathrm{d}\Gamma \right) P_j = \sum_{j=1}^{n} \left(\int_{\Gamma_j} \frac{\partial P}{\partial n}\,\mathrm{d}\Gamma \right) w_j \tag{12}$$

P and the normal derivative of P ($q = \partial P/\partial n$) may be written in terms of fundamental functions along each element, Γ_j, as:

$$P_j = \sum_{\alpha} \psi_\alpha P_{j\alpha} \quad \text{and} \quad q_j = \frac{\partial P_j}{\partial n} = \sum_{\alpha} \psi_\alpha q_{j\alpha} \quad (\alpha = 1, 2) \tag{13}$$

where P_j and q_j terms are P and q values on the element Γ_j; $P_{j\alpha}$ and $q_{j\alpha}$ terms are the values of P and q at the point α of the element Γ_j, and these terms are equal to each other for the constant element type. ψ_α represents the two ends of the element. If Eq. 13 is substituted into Eq. 12, then

$$\frac{1}{2} P_i + \sum_{j=1}^{n} \sum_{\alpha} P_{j\alpha} a_{ij}^{\alpha} = \sum_{j=1}^{n} \sum_{\alpha} q_{j\alpha} b_{ij}^{\alpha} \tag{14}$$

is obtained, where $a_{ij}^{\alpha} = \int_{\Gamma_j} \psi_\alpha \frac{\partial w_i}{\partial n}\,\mathrm{d}\Gamma$ and $b_{ij}^{\alpha} = \int_{\Gamma_j} \psi_\alpha w_i\,\mathrm{d}\Gamma$

Equation 14 is valid for all nodes on the boundary. The fundamental solution is applied at each node successively and a system of linear equations is obtained for the numerical model. This set of equations can be expressed in matrix form as:

$$AP = Bq \tag{15}$$

where A and B are two $n \times n$ matrices, and P and q are vectors of length n.

On each element, either P or q value is known from the boundary conditions, hence there are only n unknowns in the system of equations (Eq. 15). To introduce the boundary conditions into Eq. 15, one has to rearrange the system by moving columns of A and B from one side to the other, resulting C matrix. If the known values are written to the right-hand side, and the unknown values are taken to the left-hand side, Eq. 15 may be written as:

$$Cx = f \tag{16}$$

where x consists of unknown P and q values. f is found by multiplying the corresponding columns by the known values of P's or q's. The unknowns are a mixture of the potential and its derivative. The values of the pressure impulse P for the element nodes may be computed from the solution of Eq. 16.

The integrals in the above expressions can be calculated using numerical integration formulae (such as Gauss quadrature) for the case $i \neq j$. For the element $i = j$, fundamental solution requires a more accurate integration (higher-order integration rules or a special formula) due to singularity problems. For the case of constant elements, the integrals can be computed analytically.

5 Comparison of Numerical Results with Experiments

In order to apply the boundary element method to the wave impact problem, the dimensions of the solution domain were to be determined. The upper boundary of the solution domain was set at the wave crest (Fig. 5). Therefore, the breaking wave heights (H_b) for all test conditions were obtained during experiments from the records of a Sony TRV 320E video camera. Figure 7 shows a wave approaching the wall and deforming into the final breaker shape.

It is seen from Fig. 7 that 75 % of H_b remains above SWL. This percent was the average value for all cases. This

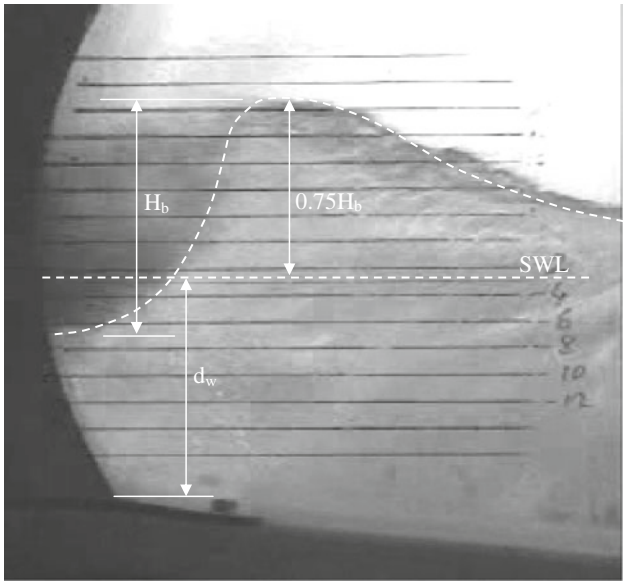

Fig. 7 Breaking shape of a wave approaching the wall

situation is compatible with the test results of Wood [39]. The height of the upper boundary from the bottom of the wall (h) is computed as follows:

$$h = d_w + 0.75H_b \tag{17}$$

where h is the height of solution domain from the bottom to the top of the wave crest at the curved wall, d_w is STL in front of the structure and H_b is the breaker height. h was calculated with the values of H_b and d_w from Table 1. It would result in velocities of about 1.5–1.7 m/s, and this observation is compatible with the results of other researchers, such as Lugni et al. [40]. The horizontal wave velocity was about 1.8 m/s in their experiments.

Wave impact experiments on the curved wall were conducted using four different radii of curvatures: $r = 30$, 40, 60, and 80 cm. For each wall, the wave heights required to create breaking wave shapes were established initially through video records. The impact pressure histories from transducers were stored. By analysing both the video records and the pressure histories, the breaker height (H_b), and the rising time (t_m) of experimental impact pressures were determined. In all cases, the impulsive pressure caused by an impact had a minimum duration of ~4 ms. Although the waves in each sample were nominally identical, their impact behaviour varied significantly. An example of the non-dimensionalized impact pressure rising time, t_m/T, from the pressure measuring devices on the walls for a typical wave impact is given in Fig. 8.

Pressure impulse values were obtained by applying boundary element method to the solution domain. The number of elements on the wall boundary was increased in

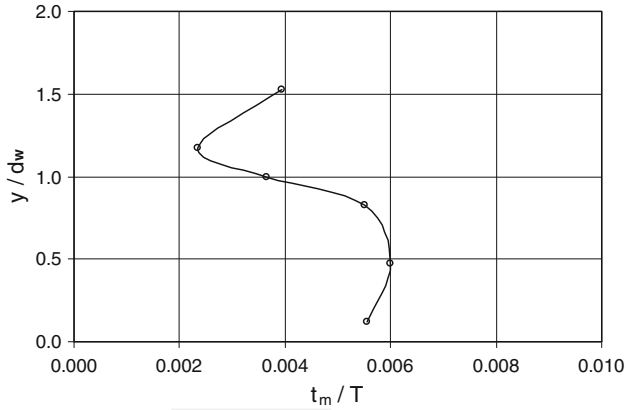

Fig. 8 An example of the non-dimensionalized impact pressure rising time t_m/T

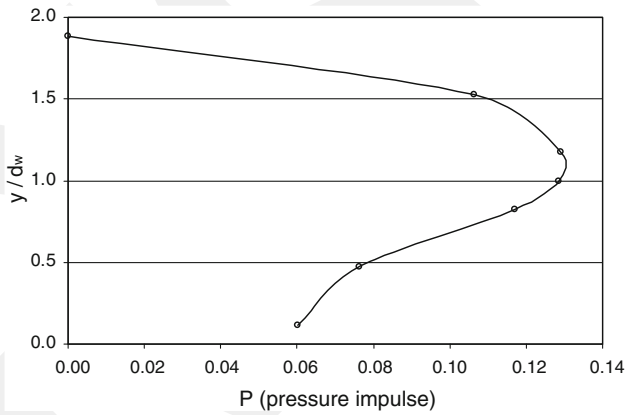

Fig. 9 A typical distribution of the pressure impulse P

order to compute the pressure impulse on the wall more precisely and also to have linear constant boundary elements. A typical distribution of the pressure impulse P over the wall height is given in Fig. 9.

The impulse values calculated from the numerical solution of Eq. 16 and the rising time (t_m) of the pressures recorded during experiments were used in Eq. 6 to compute the theoretical impact pressures.

The Bias and root mean square error (RMSE) between dimensionless theoretical and experimental impact pressures are given in Table 3. The Bias and RMSE shown in Table 3 are defined as follows:

$$\text{Bias} = \frac{1}{N}\sum_{i=1}^{N}\left[\left(\frac{p_m}{\gamma H_b}\right)_{i_{\text{theoretical}}} - \left(\frac{p_m}{\gamma H_b}\right)_{i_{\text{experimental}}}\right] \tag{18}$$

$$\text{RMSE} = \sqrt{\frac{1}{N}\sum_{i=1}^{N}\left[\left(\frac{p_m}{\gamma H_b}\right)_{i_{\text{theoretical}}} - \left(\frac{p_m}{\gamma H_b}\right)_{i_{\text{experimental}}}\right]^2} \tag{19}$$

in which N is the number of data.

Table 3 Bias and RMSE statistics of dimensionless theoretical and experimental impact pressures

Radius of curvature	BIAS			RMSE		
	$d_w = 14$ cm $H_b = 13$ cm	$d_w = 15$ cm $H_b = 14$ cm	$d_w = 17$ cm $H_b = 16$ cm	$d_w = 14$ cm $H_b = 13$ cm	$d_w = 15$ cm $H_b = 14$ cm	$d_w = 17$ cm $H_b = 16$ cm
$r = 30$ (cm)	–0.677	–0.647	1.751	1.363	2.251	3.280
$r = 40$ (cm)	1.273	0.509	1.022	1.862	1.154	3.376
$r = 60$ (cm)	0.545	0.257	3.665	1.339	2.382	5.199
$r = 80$ (cm)	–0.419	–0.012	0.827	1.096	1.328	2.377

For three different water depths ($d_w = 14$, 15, and 17 cm), theoretical and experimental impact pressures and their distribution on curved walls having different radii of curvatures are presented non dimensionally in Figs. 10, 11 and 12. The impact point for the water depths, $d_w = 14$ and 15 cm, occurred above the SWL which coincides with the pressure transducer P4. For $d_w = 17$ cm, the impact point was observed above the SWL at the pressure transducer P5.

It can be observed from Figs. 10, 11 and 12 that theoretical and experimental impact pressures on the curved walls show fairly good agreements. From past investigations, the point of maximum pressures depends on different factors such as the distance of the breaker point to the wall, the height of incoming wave, the foreshore slope and geometry, the wave period or wave length, moreover it is generally acknowledged that the maximum impact pressures on a plane vertical wall occur in the vicinity of the SWL. However, Kirkgöz [6] showed that maximum pressures on sloping walls may be above STL. In addition, the finding of Hull and Müller [10] for which the impact point for a flip-through event occurs above SWL is verified. Also in this study, the location of maximum impact pressures appears above SWL for all cases tested during the experiments as seen in Figs. 10, 11 and 12. From the comparisons of theoretical and experimental results of wave impact pressures given in Figs. 10, 11 and 12, it may be stated that the pressure impulse modelling can be used for determining the impact pressures on curved walls using the experimental rising time (t_m) values.

As seen in Figs. 10, 11 and 12, there is a slight decrease in pressures for increasing radii of curvatures, especially for the case $d_w = 14$ cm. However, Kortenhaus et al. [41] observed that pressures for increasing curvature do not necessarily increase. This situation mainly depends on the air pocket trapped between the wave and the structure. In the present study, it was not possible to determine accurately the dimensions of an air pocket. On the other hand, Bagnold [12] and Hattori et al. [26] showed that the greatest impact pressures occured when the breaking wave trapped a very thin pocket of air, although Oumeraci et al. [42] demonstrated that a plunging breaker which trapped a large air pocket could also generate high pressures. This factor needs to be evaluated further.

6 Conclusions

Laboratory tests were carried out to measure the magnitude and distribution of impact pressures caused by breaking waves on curved seawall models having different radii of curvatures. Theoretical analysis of wave impact pressures on seawalls was conducted using the pressure impulse theory. The governing equation of the problem was solved by the method of boundary elements.

The theoretical and experimental studies carried out during this study have some limitations of tests performed (regular waves, constant wave period, constant slope 1:10), and have the assumptions in setting up the numerical model and the boundary conditions (no air pocket, constant velocity, wave celerity at the wall). Depending on the limitations and assumptions mentioned above, the main conclusions from the theoretical and experimental model studies can be summarized as follows:

(a) Theoretical impact pressures and their distribution obtained using the pressure impulse model showed fairly good agreement with experimental data.
(b) The present study has clearly shown that the location of the maximum impact pressure (p_{max}) was found to occur above the SWL for all cases tested during the experiments.
(c) The pressure impulse modelling can be used for determining the impact pressures on curved walls using the experimental rising time (t_m) values.
(d) Impact pressures decrease slightly for increasing radii of curvatures, especially for the case $d_w = 14$ cm. However, a general judgement could not be put forward for the cases $d_w = 15$ and 17 cm. This situation mainly depends on the air pocket trapped between the wave and the structure. In the present study, it was not possible to determine accurately the dimensions of an air pocket. This factor needs to be evaluated further.

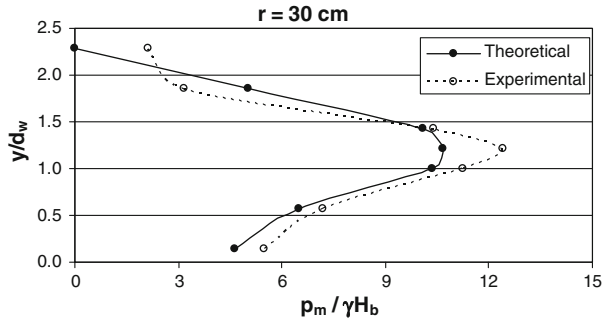

(a) r=30 cm, d_w=14 cm, H_b=13 cm

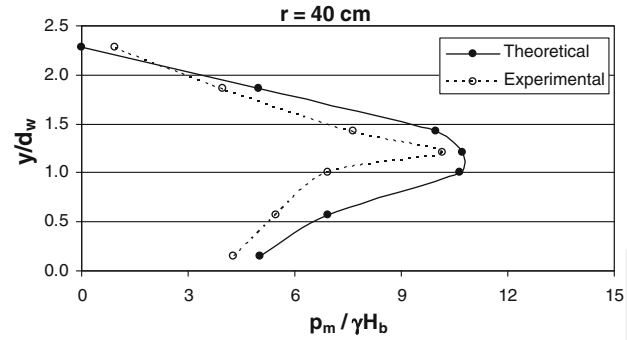

(b) r=40 cm, d_w=14 cm, H_b=13 cm

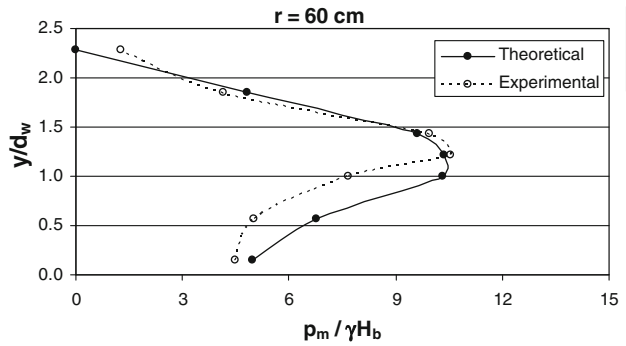

(c) r=60 cm, d_w=14 cm, H_b=13 cm

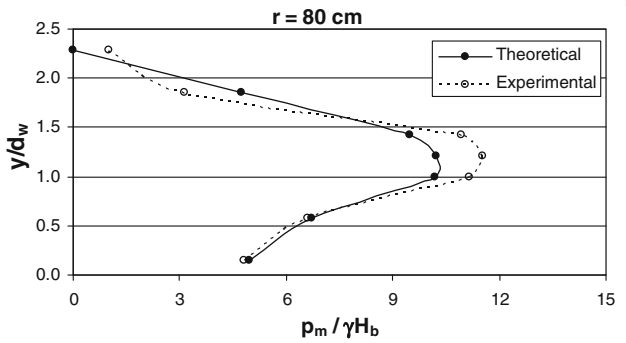

(d) r=80 cm, d_w=14 cm, H_b=13 cm

Fig. 10 Vertical distribution of theoretical and experimental impact pressures on the wall ($d_w = 14$ cm, $H_b = 13$ cm)

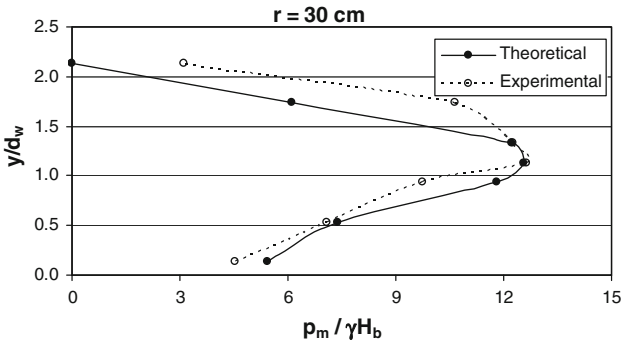

(a) r=30 cm, d_w=15 cm, H_b=14 cm

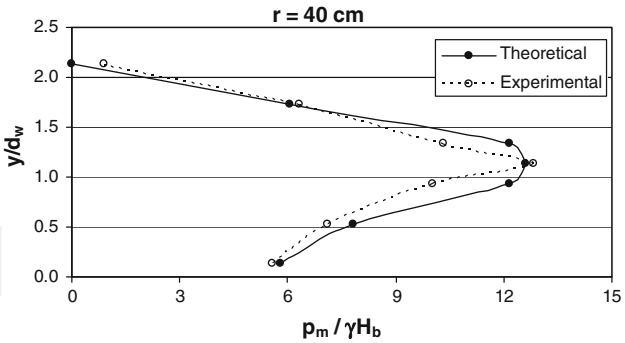

(b) r=40 cm, d_w=15 cm, H_b=14 cm

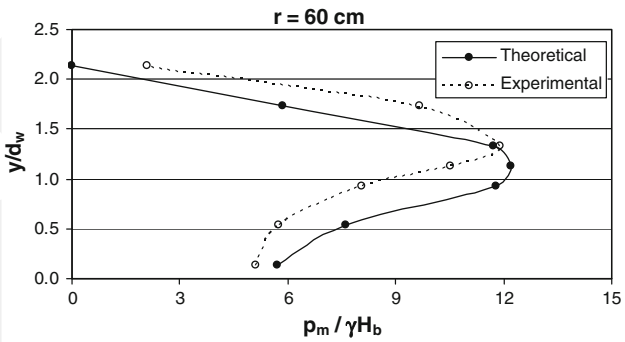

(c) r=60 cm, d_w=15 cm, H_b=14 cm

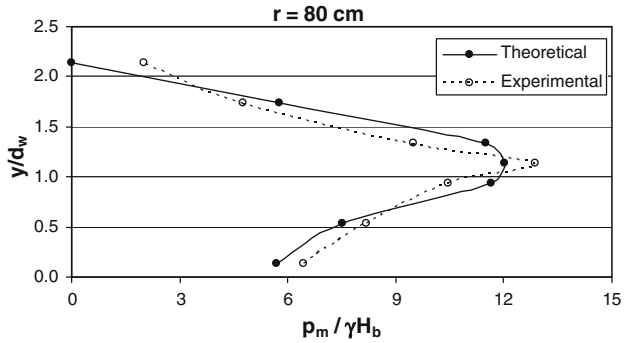

(d) r=80 cm, d_w=15 cm, H_b=14 cm

Fig. 11 Vertical distribution of theoretical and experimental impact pressures on the wall ($d_w = 15$ cm, $H_b = 14$ cm)

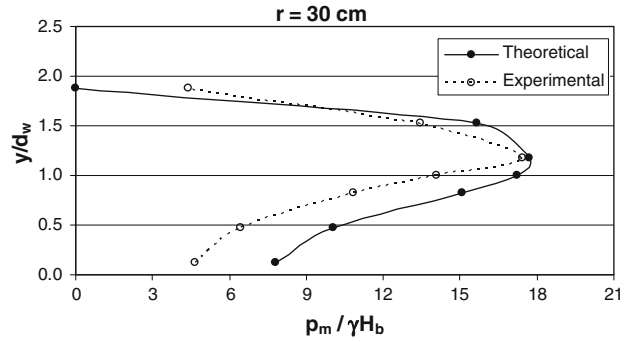

(a) r=30 cm, d_w=17 cm, H_b=16 cm

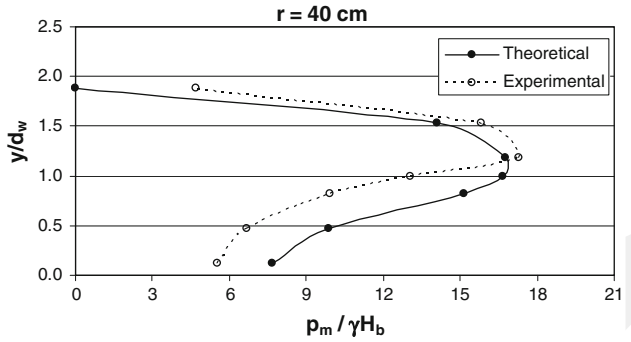

(b) r=40 cm, d_w=17 cm, H_b=16 cm

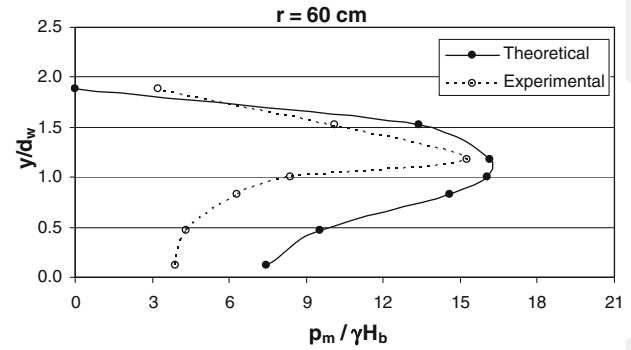

(c) r=60 cm, d_w=17 cm, H_b=16 cm

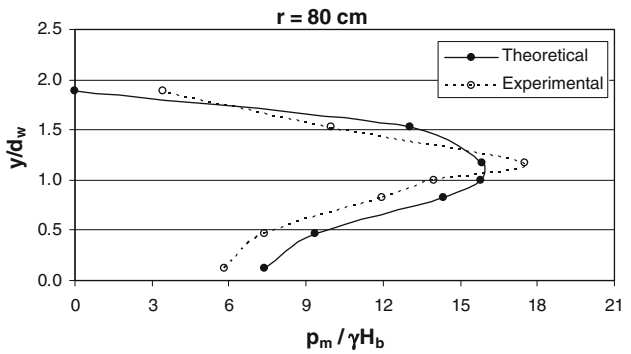

(d) r=80 cm, d_w=17 cm, H_b=16 cm

Fig. 12 Vertical distribution of theoretical and experimental impact pressures on the wall ($d_w = 17$ cm, $H_b = 16$ cm)

References

1. Peregrine, D.H.: Water-wave impacts on walls. Annu. Rev. Fluid Mech. **35**, 23–43 (2003)
2. Blackmore, P.A.; Hewson, P.J.: Experiments on full scale wave impact pressures. Coast. Eng. **8**, 331–346 (1984)
3. Partenscky, H.W.: Neue Bemessungskriterien für senkrechte und geschüttete Wellenbrecher. Jahrbuch der Hafenbautechnischen Gesellschaft, Hamburg **42**, 233–254 (1987)
4. Chan, E.S.; Melville, W.K.: Deep-water plunging pressures on a vertical plane wall. Proc. Roy. Soc. Lond. A **417**, 95–131 (1988)
5. Kirkgöz, M.S.: Shock pressure of breaking waves on vertical walls. J. Waterway Port Coast. Ocean Div. ASCE **108**, 81–95 (1982)
6. Kirkgöz, M.S.: Impact pressure of breaking waves on vertical ond sloping walls. Ocean Eng. **18**, 45–59 (1991)
7. Kirkgöz, M.S.: Breaking wave impact on vertical and sloping coastal structures. Ocean Eng. **22**(1), 35–48 (1995)
8. Neelamani, S.; Schüttrumpf, H.; Muttray, M.; Oumeraci, H.: Prediction of wave pressures on smooth impermeable seawalls. Ocean Eng. **26**, 739–765 (1999)
9. Bullock, G.N.; Crawford, A.R.; Hewson, P.J.; Walkden, M.J.A.; Bird, P.A.D.: The influence of air and scale on wave impact pressures. Coast. Eng. **42**, 291–312 (2001)
10. Hull, P.; Müller, G.: An investigation of breaker heights, shapes and pressures. Ocean Eng. **29**, 59–79 (2002)
11. Kirkgöz, M.S.; Mamak, M.: Impulse modelling of wave impact pressures on vertical walls. Ocean Eng. **31**, 343–352 (2004)
12. Bagnold, R.A.: Interim report on wave pressure research. Proc. Inst. Civil Eng. **12**, 201–226 (1939)
13. Richert, G.: Experimental investigation of shock pressures against breakwaters. In: Proceedings of International Conference on Coastal Engineering, ASCE, London, pp. 954–973 (1968)
14. Chan, E.S.: Mechanics of deep water plunging-wave impacts on vertical structures. Coast. Eng. **22**, 115–133 (1994)
15. Goda, Y.: New wave pressure formulae for composite breakwaters. In: Proceedings of the 14th Conference on Coastal Engineering, ASCE, Copenhagen, pp. 1702–1720 (1974)
16. Goda, Y.: Dynamic response of upright breakwaters to impulsive breaking wave forces. Coast. Eng. **22**, 135–158 (1994)
17. Goda, Y.: Japan's design practice in assessing wave forces on vertical breakwaters. In: Kobayashi, N.; Demirbilek, Z. (eds.) Wave Forces on Inclined and Vertical Wall Structures, pp. 140–155. ASCE, New York (1995)
18. Allsop, N.W.H.; Vicinanza, D.; Mckenna, J.E.: Wave forces on vertical and composite breakwaters. Strategic Research Report. Hydraulic Research Wallingford, SR443, Wallingford (1996)
19. Allsop, N.W.H.; Mckenna, J.E.; Vicinanza, D.; Whittaker, T.T.J.: New design methods for wave impact loadings on vertical breakwaters and seawalls. In: Proceedings of the 25th Conference on Coastal Engineering, pp. 2508–2521. ASCE, Orlando (1996)
20. Müller, G.; Whittaker, T.J.T.: An evaluation of design wave impact pressures. J. Waterway Port Coast. Ocean Eng. ASCE **122**(1), 55–58 (1996)
21. Kortenhaus, A.; Oumeraci, H.: Classification of wave loading on monolithic coastal structures. In: Proceedings of the 26th Conference on Coastal Engineering, pp. 867–880. ASCE, Copenhagen (1998)
22. Goda, Y.: Random Seas and Design of Maritime Structures, 2nd edn. World Scientific, Singapore (2000)
23. Cuomo, G.; Allsop, N.W.H.: Wave impacts at seawalls. In: Proceedings of the 29th Conference on Coastal Engineering, pp. 4050–4062. World Scientific, Lisbon (2004)
24. Kamikubo, Y.; Murakami, K.; Irie, I.; Hamasaki, Y.: Study on practical application of a non-wave overtopping type seawall.

In: Proceedings of the 27th Conference on Coastal Engineering, pp. 2215–2228. ASCE, Sydney (2000)
25. Yamashiro, M.; Yoshida, A.; Irie, I.: Development of non-wave overtopping type seawall in deepwater. In: Proceedings of the 29th Conference on Coastal Engineering, pp. 4367–4378. World Scientific, Lisbon (2004)
26. Hattori, M.; Arami, A.; Yui, T.: Impact wave pressure on vertical walls under breaking waves of various types. Coast. Eng. **22**, 79–114 (1994)
27. Bullock, G.N.; Obhrai, C.; Peregrine, D.H.; Bredmose, E.H.: Violent breaking wave impacts. Part 1: results from large-scale regular wave tests on vertical and sloping walls. Coast. Eng. **54**, 602–617 (2007)
28. Wood, D.J.; Peregrine, D.H.; Bruce, T.: Wave impact on a wall using pressure impulse theory I: Trapped air. J. Waterway Port Coast. Ocean Eng. ASCE **126**(4), 182–190 (2000)
29. Shimosako, K.; Takahashi, S.: Application of expected sliding distance method for composite breakwaters design. In: Proceedings of the 27th International Conference on Coastal Engineering, pp. 1885–1898. ASCE, Sydney (2000)
30. Carr, J.H.: Breaking wave forces on plane barriers. Contract No-12561, Report No. E-11.3. Hydrology Laboratory of California Institute of Technology, Pasadena, California (1954)
31. McKenna, J.E.; Allsop, N.W.H.: Statistical distribution of horizontal wave forces on vertical breakwaters. In: Proceedings of the 26th Conference on Coastal Engineering, pp. 2082–2095. ASCE, Copenhagen (1998)
32. Cooker, M.J.; Peregrine, D.H.: Pressure-impulse theory for liquid impact problems. J. Fluid Mech. **297**, 193–214 (1995)
33. Rouville, A.; Besson, P.; Petry, P.: Etat actuel des études intemationales sur les efforts dus aux lames. Ann. Ponts Chaussées **108**(I1), 5–113 (1938)
34. Nagai, S.: Shock pressures by breaking waves on breakwaters. J. WatWay Harbors Div. ASCE **86**, 1–38 (1960)
35. Mitsuyasu, H.: Shock pressure of breaking waves I. Coastal Eng. Japan **9**, 83–96 (1966)
36. Kirkgöz, M.S.: Breaking waves: their action on slopes and impact on vertical seawalls. Ph.D. thesis, University of Liverpool, UK (1978)
37. Mamak, M.: Wave forces on curved seawalls. PhD thesis, Çukurova University, Adana, Turkey (in Turkish) (2002)
38. Brebbia, C.A.; Dominguez, J.: Boundary Elements: An Introductory Course. Computational Mechanics Publications, Southampton (1989)
39. Wood, A.M.M.: Coastal Hydraulics, p. 136. Gordon and Breach, New York (1969)
40. Lugni, C.; Brocchini, M.; Faltinsen, O.M.: Wave impact loads: the role of the flip-through. Phys. Fluids **18**, 122101-17 (2006)
41. Kortenhaus, A.; Haupt, R.; Oumeraci, H.: Design aspects of vertical walls with steep foreland slopes. In: Proceedings of Breakwaters, Coastal Structures and Coastlines, London (ICE), pp. 221–232 (2001)
42. Oumeraci, H.; Bruce, T.; Klammer, P.; Easson, W.J.: PIV measurements of breaking wave kinematics and impact loadings on caisson breakwaters. In: 4th International Conference on Port Engineering in Developing Countries, Rio de Janerio, vol. 3, pp. 2394–2410. Brazilian Water Resources Association, Brazil (1995)